33rd Annual International Conference of the IEEE EMBS
Boston, Massachusetts USA, August 30 - September 3, 2011

Automatic Vessel Segmentation in Wide-field Retina Images of Infants with Retinopathy of Prematurity

Enea Poletti, Diego Fiorin, Enrico Grisan, *Member IEEE*, and Alfredo Ruggeri, *Senior Member, IEEE*

***Abstract*—The earliest signs of Retinopathy of Prematurity (ROP) are tortuosity and dilation of retinal vessels. Such vascular changes are considered of primary importance for the diagnosis and the follow-up of the disease. However, a widely accepted computerized system for their quantitative measurement is still missing.**

Images taken from a preterm baby's eye are often low-contrast, noisy, and blurred. Algorithms that have been successfully applied to analyze adult retinal images do not work well in ROP images. We propose here a novel method for the automatic extraction of vessel centerline in wide-field ROP retinal images, based on a sparse tracking scheme. After a set of seed points is identified all over the image, vessels are traced by connecting those seeds by means of minimum cost paths, whose weights depend on similarity features and alignment evaluated by a custom line operator.

The performance of the method was assessed on a dataset of 20 images acquired with the RetCam fundus camera. A sensitivity of 0.78 and a false detection rate of 0.15 were obtained with respect to manual ground truth reference.

I. Introduction

Retinopathy of Prematurity (ROP) [1] is an serious eye disease that affects prematurely born babies. It can be mild and resolve spontaneously, but in more serious cases it become very aggressive: new blood vessel formation progresses to scarring, retinal detachment and blindness.

Regional shortages in the availability of ophthalmologists able to provide ROP diagnostic examinations are a substantial barrier to ensuring worldwide appropriate ROP care. One solution would be to perform a wide screening with retinal photography, an alternative to manual direct ophthalmology, and automatizing the image assessment. Wide-field retinal cameras (130^o of field of view, e.g., RetCam by Clarity Medical Systems, CA, USA) are recent commercially available devices that allow inspecting the most peripheral area of the eye, where vessels grow during the last weeks of gestation. Several studies have evaluated its clinical value in screening for ROP [2]. However, the unavailability of effective automated analysis tools and of quantitative clinical grading procedures is at present limiting their circulation.

Fig. 1. Two examples of wide-field ROP Image.

The earliest signs of ROP are increased tortuosity and dilation of retinal vessels. Such vascular changes are considered of primary importance for the diagnosis and the choice of treating option for the disease. At the present, however, these signs are evaluated only qualitatively, by subjective visual inspection. Clinical availability of specific algorithm for image analysis would allow the quantitative and objective evaluation of the occurrence of these signs.

The main drawbacks of RetCam images (Fig. 1), with respect to images provided by standard adults fundus cameras, are: 1) low contrast, 2) presence of interlacing artifacts, as images are actually single frames extracted from video, 3) narrow blood vessels, due to the wide-field of view coupled with the 640x480 pixel resolution, 4) non uniform illumination in the captured wide field of view, 5) high visibility of choroidal vessels, related to the lack of pigmentation of the

Manuscript received April 15, 2011.

All authors are with the Department of Information Engineering, University of Padua, Padua, Italy (corresponding author: Alfredo Ruggeri; phone: +39 049 827 7624; fax: +39 049 827 7699; e-mail: alfredo.ruggeri@ unipd.it).

infant choroid. All these aspects make the automatic analysis of RetCam images quite challenging and custom techniques are therefore necessary to successfully trace the vasculature.

II. Material

Twenty RetCam images, with 120° field of view and 640x480 pixels size, were acquired in premature babies at different stages of ROP and provided by Clarity Medical Systems, CA, USA. A manual segmentation of the vessel network was provided by two of the authors (DF and EP) and used to evaluate the performance of the algorithm proposed for vessel extraction.

III. Methods

The rationale of the proposed method is to effectively combine the modified versions of two different techniques ([3] and [4], [5]) that individually proved to be unable to properly deal with wide-field ROP image features.

After a preliminary de-interlacing process (sec. III-A), a set of seed points is identified over the whole image (sec. III-B). In order to enhance the true vessels and discard the choroidal ones, four *oriented line strength components* are extracted (sec. III-C): they are employed by the subsequent algorithm, which evaluates the minimum cost paths connecting the seeds (sec. III-D, D1, D2), so as to robustly discriminate retinal vessels against choroidal ones.

A. Preliminary Image Enhancement

As previously mentioned, during acquisition the RetCam fundus camera records a video. The images taken into consideration are manually selected video frames that present a good contrast between vessels and background. Because frames are affected by interlacing artifacts (Fig. 2a) due to the motion of infant eyes, a de-interlacing algorithm is employed to recover a better quality image.

In interlaced mode, two sub-images I_O and I_E, containing respectively the odd and the even horizontal lines, are acquired by the camera. In the de-interlacing algorithm, the missing lines of I_O and I_E (i.e. the even and the odd lines, respectively) are recovered by interpolation, obtaining I_O^I and I_E^I. I_O^I and I_E^I are then aligned by maximizing the 2-dimension correlation coefficient, obtaining a rigid registration. The final de-interlaced image I_D is composed by the odd and even lines of I_O^I and I_E^I respectively (Fig. 2b).

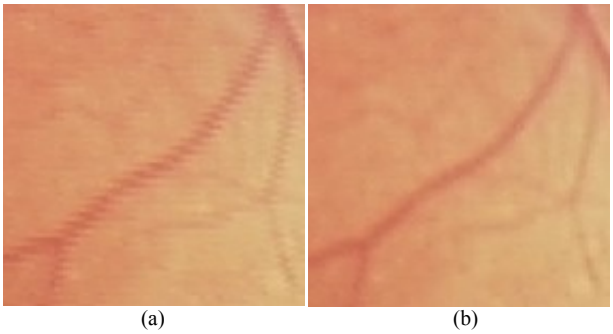

(a) (b)

Fig. 2. A detail of a frame (a) before de-interlacing and (b) after.

B. Seed Point Extraction

The objective of this step is to extract a set of points (seeds) from which the vessel tracking procedure will start. A number of equally spaced rows and columns of the image are analyzed. From each selected line, the gray-level profile is extracted and analyzed, looking for patterns corresponding to candidate vessels: the profile is convolved with a discretized Laplacian of Gaussian filter over multiple scales and the maximum response among the output results is considered [3]. The difference between background and vessels along the profile is maximized when the grid lines are perpendicular to the vessels. Hence, in order to improve the seed extraction procedure, we decided to use two regular grids: one of equally spaced rows and columns and a similar one rotated by 45°.

C. Oriented line strength component

The line operator principle was first described in [4] and [5]. The average grey-level L of the pixels lying on a line passing through the target pixel is calculated for multiple orientations and the orientation yielding the largest value, L_{max}, is chosen. The line-strength S is given by $L_{max} - M$ where M is the average grey-level of a similarly oriented square neighborhood.

In our implementation, 12 oriented 15-pixel lines are used (see examples in Fig. 3) and the square window is not oriented like the corresponding line but it is kept fixed like in [6], where the line operator is used to extract features for a supervised classifier.

Differently from the original methods, however, we do not consider the single line strength resulting from all the twelve orientations, but only the four line strength components that

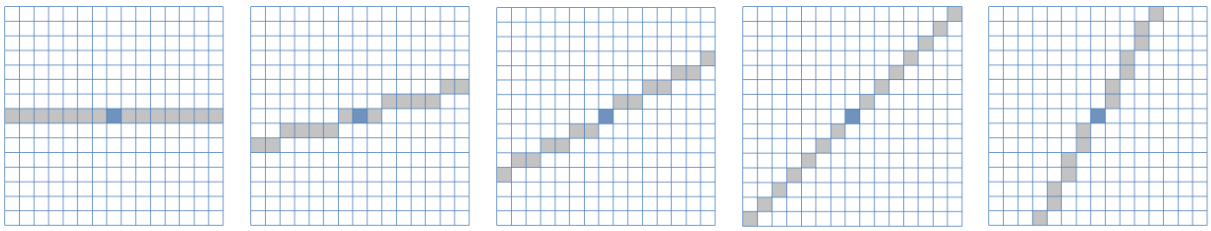

(a) (b) (c) (d) (e)

Fig. 3. Single line operators at the orientation of (a) 0°, (b) 15°, (c) 30°, (d) 45°, and (e) 60°.

correspond to the four orientations $\vartheta \in \{0°, 45°, 90°, 135°\}$ as:

$$S_\vartheta = \max\left\{L_\varphi \mid \varphi \in \{\vartheta - 15°,\ \vartheta,\ \vartheta + 15°\}\right\} - M \quad (1)$$

Following Eq. 1, the line strength at the orientation of 0°, $S_{0°}$, is computed by evaluating the maximum response amongst the line oriented at 345°, 0°, and 15°. The four partial line strength components are considered, instead of the total one used in [6], because they work in the most advantageous way with the tracking algorithm described in sec. III-D, allowing a better discrimination between actual vessels and choroidal vessels.

The computational time required by the filtering is very low because every single pixel of the image is convolved with only 12 masks. Moreover, the average grey level of lines is not obtained by interpolation, but the pixels of the line operator are found by rounding the coordinates of an ideal line.

D. Vessel Tracking

The rationale of the tracking method is to consider the image as a weighted unoriented sparse graph where each node represents a pixel. The graph edges describe the 8-adjacency among pixels in the image. Under the assumption that vessels are minimum cost paths connecting remote nodes, we employ a graph search approach in order to identify them [3].

An undirected graph is derived from the original image. The scheme of the proposed algorithm is to run in parallel multiple instances of shortest path searches *à la* Dijkstra [7], each starting from the nodes/pixels that have been identified as seeds. Every shortest path search is described by a searching tree, which evolves though iterations by exploring new areas of the image. When two search trees meet, the shortest path connecting their roots is obtained. Then these two trees merge into a single new tree, from which the search goes on in successive iterations.

D1. Exploration

The first operation is to initialize all the structures needed to keep the required information. A distance value equal to zero is assigned the seed nodes, equal to infinity for all other nodes. All nodes are marked as *unexplored*, which means that they are enabled to be considered by the exploration process in future iterations.

Then, a different searching tree starts expanding from each single seed node. The algorithm has an iterative structure. At each iteration:

- the *unexplored* node a with the minimum distance value is considered;
- the *unexplored* neighbors $\{b_i\}$ of a are considered;
- if there is a b_k belonging to a tree different from the tree of a, these two trees are merged and the minimum path connecting their roots is reconstructed;
- otherwise, for every neighbor b_i, its distance value is calculated by evaluating the cost function $f(a, b_i)$ (see sec. III-D2);
- if this distance is less than the one previously recorded in b_i, the old distance is replaced by the new;
- a is marked as *explored*: it will not be considered ever again.

The algorithm ends when there is no tree that merged after a fixed number of iterations.

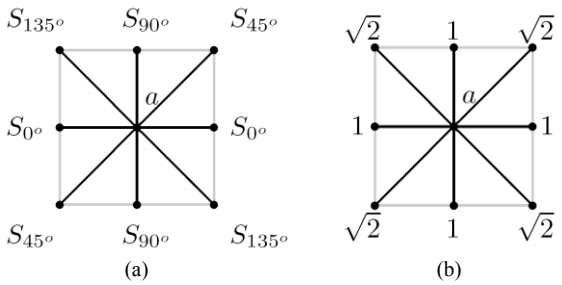

Fig. 4. (a) Terms $\boldsymbol{S}$ and (b) $\boldsymbol{w}$ of $\boldsymbol{f(a,b)}$ depend on the adjacency between $\boldsymbol{a}$ and its neighbors.

D2. The Cost Function

We defined the cost function f associated to the edge (a, b) as:

$$f(a,b) = c_1\, d_a + \left(g_{a,b} + S_{\vartheta(a,b)}\right) w_{a,b} \quad (2)$$

where d_a is the distance recorded in the node a; c_1 is a weighting coefficient; $g_{a,b}$ is related to the gray intensity of the image; and $w_{a,b}$ and $S_{\vartheta(a,b)}$ are related to the orientation of b in respect to a (Fig. 4);

$$g_{a,b} = c_2\ \mathrm{glvl}(a) + c_3\ |\mathrm{glvl}(a) - \mathrm{glvl}(b)| \quad (3)$$

where $\mathrm{glvl}(a)$ is the gray level of the pixel associated to the node a, and c_2 and c_3 are two weighting coefficients empirically set.

$$w_{a,b} = \begin{cases} 1, & \text{if } a \text{ and } b \text{ are } 4-\text{adjiacent} \\ \sqrt{2}, & \text{if } a \text{ and } b \text{ are } \mathrm{d}-\text{adjiacent} \end{cases} \quad (4)$$

The value of $S_{\vartheta(a,b)}$ is obtained by evaluating the particular line strength component corresponding to the angular position of the pixel b related to the node a. The line strength to be selected is $S_{0°}$ if a and b are horizontally aligned, $S_{90°}$ if a and b are vertically aligned, $S_{45°}$ or $S_{135°}$ if they are diagonally aligned by 45° or 135° respectively (
Fig. 4).

IV. Results and Discussion

The performance of the algorithm has been assessed by comparing the tracking results (Fig. 5) with the manually segmented version of the 20 images of our set, assumed as ground-truth reference. The pixels in the automatically traced vessels that belong to the background in the corresponding ground-truth images are considered false positives, whereas those belonging to a manually traced vessel are

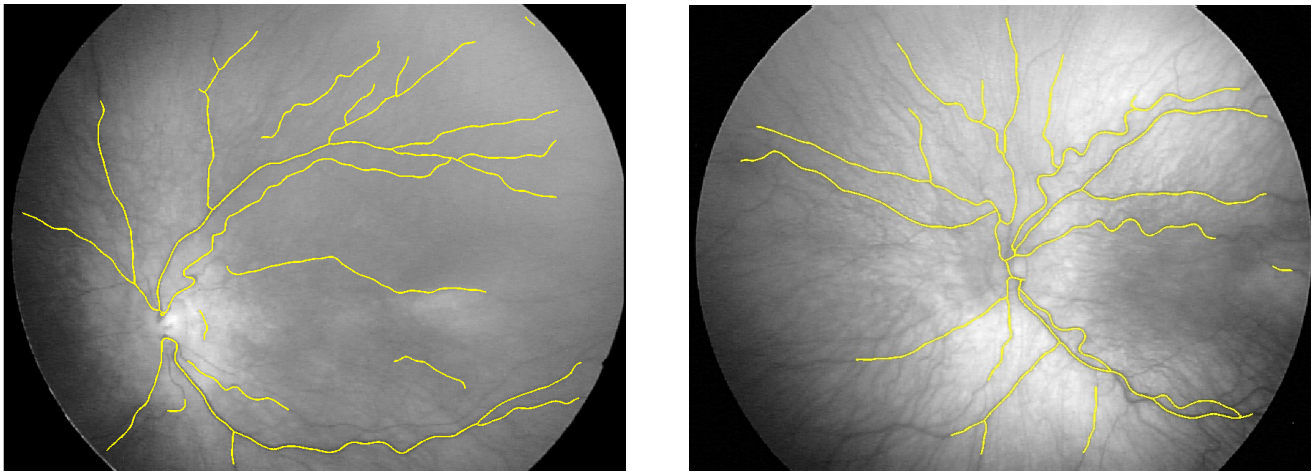

Fig. 5. Two example images of tracking result.

considered true positive. Sensitivity has been evaluated as the percent fraction of the true positive over the total number of pixels of the ground-truth vessels. False vessel detection has been evaluated as the percent fraction of the false positive over the total length of the estimated vessels (true and false positive). Results are summarized in Tab. I in terms of mean, standard deviation, minimum and maximum of both sensitivity and false vessel detection over the whole data set.

TABLE I
RESULTS OF VESSEL TRACING IN THE 20 IMAGES SET (%)

	Mean	Sd	Min	Max
Sensitivity	78.4	15.3	58.3	94.1
False detection	15.2	5.5	4.3	21.4

It is worth noting that the tracking sensitivity obtained in RetCam images is comparable to the sensitivity reached by state-of-the-art algorithms on some publicly available adult image datasets [6]. However, to the best of our knowledge, there is no public image dataset of RetCam images, so it is not possible to compare the performance of the proposed technique against other methods presented in literature. Moreover, only few algorithms were tested on wide-field infant images acquired with RetCam, and only very few authors reported quantitative performance. Heneghan et al reported very high sensitivity and specificity, but using only a very small 260 x 260 pixel selection of a typical wide-field image [8].

The high variability of the results (standard deviation and range between maximum and minimum values in Table I) is a direct consequence of the high variability in the quality of the 20 images. In fact, the dataset includes images with different contrast between vessels and background, different illumination and variable retinal transparency (leading to variable visibility of choroidal vessels).

The average run time of the Matlab® prototype on an Intel Duo 2 PC (3.0 GHz, 4 GB of RAM) was about 10 seconds.

V. CONCLUSION

RetCam retinal images acquired from newborns can be analyzed to obtain clinical indexes that could improve the diagnosis and the follow-up of ROP.

A new, fully automatic system capable to extract the vessel structure in these images, based on a minimum cost path search and line strength operators, has been described and its performance on a 20 images data set proved its robustness against the low quality that characterizes the ROP images.

The present version does not include yet a user interface that allows the editing of the results (e.g., the manual elimination of the false vessels). However, also in its present form the method proved to be adequate for vessel tracing, suggesting the possibility of its application to derive retinal vascular morphology for clinical purposes.

REFERENCES

[1] Committee for the Classification of Retinopathy of Prematurity, The International Classification of Retinopathy of Prematurity revisited. Arch Ophthalmol. 123 (2005) no. 7, 991–999.

[2] B. Lorenz, K. Spasovska, H. Elflein, et al., “Wide-field digital imaging based telemedicine for screening for acute retinopathy of prematurity (ROP). Six-year results of a multicenter field study”, Graefes Arch Clin Ophthalmol. (2009); 247(9):1251-1262.

[3] E. Poletti, D. Fiorin, E. Grisan, and A. Ruggeri, “Retinal vessel axis estimation through a multi-directional graph search approach,” in Proc. *World Congress Med. Phys. Biomed. Eng*., vol. 25/11, Berlin/Heidelberg, Germany, Springer-Verlag, 2009, pp. 137–140.

[4] Marti, R., R. Zwiggelaar, et al. (2001). Automatic Registration of Mammograms Based on Linear Structures. Information Processing in Medical Imaging. M. Insana and R. Leahy, Springer Berlin / Heidelberg. 2082: 162-168.

[5] R. N. Dixon and C. J. Taylor, “Automated Asbestos Fiber Counting,” ser. Conference. Philadelphia, PA: Inst. Physics, 1979, vol. 44, pp. 178–185.

[6] Ricci, E., Perfetti, R.; , "Retinal Blood Vessel Segmentation Using Line Operators and Support Vector Classification," *Medical Imaging, IEEE Transactions on*, vol.26, no.10, pp.1357-1365, Oct. 2007

[7] E. Dijkstra, “A note on two problems in connection with graphs,” *Numerische Mathematik*, vol. 1, pp. 269–271, 1959.

[8] C. Heneghan, J. Flynn, M. O'Keefe, and M. Cahill, “Characterization of changes in blood vessel width and tortuosity in retinopathy of prematurity using image analysis”, *Med Im Anal* 6 (2002), 407-429.